

1 **Stratification and Mixed Layer Depth around**  
2 **Iceland: Characterization and inter-annual**  
3 **variability**

4 Angel Ruiz-Angulo <sup>1\*</sup>, Esther Portela <sup>2</sup>, Charly de Marez<sup>1</sup>, Andreas Macrander<sup>3</sup>,  
5 Sólveig Rósa Ólafsdóttir<sup>3</sup>, Thomas Meunier <sup>4</sup>, Steingrímur Jónsson <sup>3,5</sup>, and M. Dolores  
6 Pérez-Hernández <sup>6</sup>

7 <sup>1</sup>Earth Science Institute, University of Iceland, 101 Reykjavik, Iceland  
8 <sup>2</sup>Univ. Brest, Laboratoire d'Océanographie Physique et Spatiale, CNRS, IRD, Ifremer, Plouzané, France  
9 <sup>3</sup>Hafrannsóknastofnun / Marine and Freshwater Research Institute, Hafnarfjörður, Iceland,  
10 <sup>4</sup>Woods Hole Oceanographic Institution, Woods Hole MA, USA  
11 <sup>5</sup>University of Akureyri, Akureyri, Iceland  
12 <sup>6</sup>Unidad océano y clima, Instituto de Oceanografía y Cambio Global, IOCAG, Universidad de Las Palmas de Gran Canaria,  
13 ULPGC, Unidad Asociada ULPGC-CSIC, Las Palmas de Gran Canaria, Spain

14 *Correspondence to:* Angel Ruiz-Angulo (angel@hi.is)

15 **ABSTRACT**

16 The ocean around Iceland is a key region where major water masses and currents interact, influencing the global ocean  
17 circulation. Here, we analyze 29 years (1990-2019) of quarterly hydrographic section data collected around Iceland. The  
18 hydrographic properties around Iceland show important spatial variability. Based on temperature, salinity, and stratification  
19 structure, we classified the Icelandic waters in three distinct regions: the south, the north and northeast regions. The warm  
20 and salty Atlantic Waters that dominate the south show the deepest winter mixed layers (~500m) while the north and  
21 northeast show shallower depths (~100m). Based on the decomposition of total stratification into temperature and salinity  
22 contributions, we find that, the subsurface stratification is mainly controlled by temperature in the south, by salinity in the  
23 northwest, while in the north, the North Icelandic Irminger Current and East Icelandic Current alternate seasonally, shifting  
24 the region between temperature-dominated and salinity-dominated stratification. The interannual variability of the mixed  
25 layer and of its thermohaline properties is also large around Iceland. Mixed layer waters were generally colder in the 90's,  
26 then warmed until approximately 2015, and became colder again from 2015 to 2018. In the northeast, a multidecadal mixed  
27 layer warming trend emerges from the interannual variability as the Atlantic Water progresses northeastward, which is  
28 responsible for transforming locally the upper stratification from salinity-dominated into temperature-dominated. This is  
29 associated with the "Atlantification" of the Arctic. Within the mixed layer south of Iceland, density has continuously  
30 decreased since the mid 1990's. Elsewhere, we observe density-compensated changes in mixed layer temperature and  
31 salinity, without clear long trends. This study provides an unprecedented and detailed description of the seasonal to multi-  
32 decadal variability of the mixed layer depth and stratification around Iceland, showing links between this regional  
33 variability and changing North Atlantic under global warming.

34 **Keywords:** Mixed layer depth, Mixed layer properties, stratification, Ocean warming, Atlantification, Interannual  
35 variability

36

Deleted: ,

Deleted: c

Deleted: witnesses some of the most important transformations...

Deleted: of

Deleted: that drive

Deleted: S

Deleted: N

Deleted: N

Deleted: S

Deleted: N

Deleted: N

Deleted: S

Deleted: N

Deleted: N

Deleted: N

Deleted: clear

Deleted: clearly

Deleted:

Deleted:

Deleted: , allowing for the formation of deeper mixed layers

Deleted:

Deleted:

60 1 INTRODUCTION

61 The ocean around Iceland is a key region where major water masses and currents interact, shaping the North Atlantic  
62 circulation and play a crucial role on the Atlantic Meridional Overturning Circulation (AMOC). The Nordic Seas are among  
63 the few places on the globe where the formation of deep waters (1000-3000 m depth) occurs during winter deep convection  
64 (Petit et al., 2020). The southern end of the Nordic Seas is bounded by the Greenland-Iceland-Scotland Ridge (GISR). The  
65 North Atlantic Current (NAC) brings the warm and salty Atlantic Water (AW) northward into the Nordic Seas (Hátún and  
66 Chafik, 2018; Østerhus et al., 2019; Hátún et al., 2021). The AW crosses the ridge in three ways (Fig. 1): (i) between  
67 Greenland and Iceland, where the Irminger Current (IC) forms the North Icelandic Irminger Current (NIIC) bringing AW  
68 that flows clockwise around Iceland (Jónsson & Briem, 2003; Jónsson & Valdimarsson, 2012); (ii) between Iceland and  
69 the Faroe Islands (Mauritzen, 1996); and (iii) through the Faroe Shetland Channel (Hansen and Østerhus, 2000; Hansen et  
70 al., 2023), contributing up to 48% of the total AW transport. The AW undergoes strong cooling and densification in the  
71 Nordic Seas and the Arctic Ocean (Mauritzen, 1996; Pérez-Hernández et al., 2019; Athanase et al., 2020; Huang et al.,  
72 2023). This modified AW is referred to as Atlantic-origin Overflow Water (AtOW; e.g., Havik et al., 2017; Casanova-  
73 Masjoan et al., 2020) and is one of the two sources of Denmark Strait Overflow Water (DSOW; Semper et al. 2019). AtOW  
74 travels southward as a mid-depth water mass in the East Greenland Current (EGC; Håvik et al., 2017), from where, part of  
75 it diverts east and merges with the NIIC northeast of Iceland (Casanova-Masjoan et al., 2020).

76 The transformation of AW into AtOW takes place in different areas of the Nordic Seas: along the Norwegian Current  
77 (Håvik et al., 2017), in the Iceland Sea Gyre (Våge et al., 2013), on the eastern side of Greenland, or even -due to its  
78 proximity- in the Arctic Basin (Pérez-Hernández et al., 2019). This transformation has different driving mechanisms  
79 impacting mixing and convective processes. Wind-stress, sea-ice retreat and high heat loss due to cold-air outbreaks drives  
80 the transformation east of Greenland (Våge et al., 2018), sea-ice retreat and heat exchange dominate north of Svalbard  
81 (Pérez-Hernández et al., 2019; Athanase et al., 2020), and heat fluxes are the main drivers in the center of Iceland Sea  
82 (Våge et al., 2013). Thus, the Nordic Seas region has been previously described as a “mixing pot” (Renfrew et al., 2019),  
83 largely responsible for the overall formation of deep overflow water (Lozier et al., 2019). The Nordic Seas are also a large  
84 repository of freshwater, primarily originated from glacier melt and river discharge. This water mass increases buoyancy  
85 and is carried southward by the East Greenland Current (EGC). Therefore, it is crucial to fully understand the variability  
86 of the upper ocean, where mixed layers (ML) develop and transform these water masses.

87 The Arctic Ocean is warming much faster than the global average, a process known as “Arctic Amplification,” which is  
88 also associated with the “Atlantification” of the Arctic (Polyakov et al., 2017; Dai et al., 2019). While the causes are still  
89 debated, Arctic Amplification has evident consequences, such as a decrease in seasonal sea-ice extent and a weakening of  
90 the cold halocline (Polyakov et al., 2020; Dai et al., 2019). Although these changes are less pronounced in the central  
91 Iceland Sea, similar processes have been observed in the central Greenland Sea and the northeastern shelf (Gjelstrup et al.,  
92 2022; Strehl et al., 2024), suggesting that Atlantification may also influence the Iceland Sea. Changes in temperature and  
93 salinity in the upper ocean modify upper-ocean stratification, which partially controls the mixed layer depth (MLD).

94 The depth and structure of the ML is primarily controlled by local buoyancy forcing, i.e., surface heat loss and freshwater  
95 fluxes, which modifies the water density (Kohler et al., 2018). For instance, within the Iceland Basin, wintertime buoyancy  
96 loss drives deep convection, shaping the thermohaline properties that influence the lower limb of the AMOC and its  
97 variability in the subpolar North Atlantic (Petit et al., 2021). The pre-existing stratification of the water column is  
98 responsible for controlling the effect of the surface forcing. Strongly stratified upper layers resist mixing, while weak  
99 stratification allows deeper penetration of turbulence and convection mixing (Pierce et al., 1986). Over shorter timescales,  
100 on the order of days, the MLD can significantly deepen as a result of the strong wind events with significant wind stress

Deleted: The Nordic Seas, together with the Irminger Sea and the Iceland Basin,

Deleted: Våge et al., 2015, 2018

Deleted: and

Deleted: drive

Formatted: Font: Not Italic

Deleted: The Nordic Seas are also a large repository of freshwater arising from glacier/river discharge and from the Arctic...

Formatted: Font: Not Italic

Deleted: The Arctic Ocean is warming much faster than the global average, a process known as the “Arctic Amplification”, which is also associated with the “Atlantification” of the Arctic (Polyakov et al., 2017; Dai et al., 2019). Even though the causes are still in debate, there are evident observed consequences of Arctic Amplification, such as a decrease in the extent of seasonal sea-ice (Dai et al., 2019) and a weakening of the cold halocline (Polyakov et al., 2020). Changes in temperature and salinity in the upper ocean modify the upper ocean stratification, which partially controls the mixed layer depth (MLD).

Formatted: Indent: Left: 0,09 cm

Deleted: Wind forcing contributes by enhancing turbulent mixing, deepening the ML under certain conditions (Petit et al., 2020). ...

23 and associated large wave heights (Skylingstad et al., 2023). MLD and stratification are strongly influenced by  
24 atmospheric forcing, including variability associated with the North Atlantic Oscillation (NAO), which modulates wind  
25 stress, surface heat flux, and freshwater input in the Iceland region (Hurrell, 1995; Dickson et al., 1996).

Deleted: ¶

126 The IPCC report indicates with *high confidence* that roughly 40% of the global ocean mean upper ocean stratification  
127 has increased about 3.3–6.1% since 1960 due to both oceans warming and high-latitude freshening (Tesdal et al., 2018;  
128 Yamaguchi and Suga, 2019; Bindoff et al., 2019; Liu et al., 2020; Sallée et al., 2021). Increased stratification is associated  
129 with less efficient diapycnal mixing, reducing the exchanges of heat and tracers from the mixed layer into the ocean interior.  
130 It has also been observed, with *high confidence*, that the ML is undergoing changes (Bindoff et al., 2019; on Climate  
131 Change, IPCC). Particularly, the shallow summertime ML, which is more likely to be affected by global warming, is  
132 deepening at a rate of 5 – 10 m per decade (Sallée et al., 2021). Despite the reported global patterns, it has been also  
133 acknowledged that regional changes might differ from the global estimates (Fox-Kemper et al., 2021).

Deleted: ocean

Deleted:

Deleted: cé

Deleted: undergoing

Deleted: e

Deleted: on Climate Change, IPCC

134 The warming of the ML and the associated increase in stratification have an impact in biogeochemical processes like  
135 phytoplankton blooms and carbon or oxygen sequestration, key components for the Earth’s climate (Olafsson, 2003; Pérez  
136 et al., 2021). In the waters surrounding Iceland, the phytoplankton community is closely linked with the water mass  
137 properties and hence, an “Atlantification” will replace Polar communities with more Atlantic communities (Cerfonteyn et  
138 al. 2023). In the Arctic Ocean, north and northwest of Iceland, the early onset of stratification in spring gives rise to rapid  
139 shallowing of the mixed layer and triggers early spring phytoplankton blooms, whereas the weakly stratified water-column  
140 in the Atlantic water and the associated deep ML delay, the spring bloom south of Iceland (Zhai et al., 2012). This also has  
141 strong consequences in carbon uptake, vertical nutrient supply and biological processes (Yamaguchi and Suga, 2019).  
142 Other indirect impacts of the increased stratification include changes in upwelling, deep-water formation rates, biological  
143 production, and remineralization rates (Holt et al., 2016), and deoxygenation (Shepherd et al., 2017).

Deleted: influence

Deleted: p

Deleted: s

Deleted: S

144 Thus, the overall goal of this study is to characterize the spatial and temporal variability of the mixed layer and  
145 stratification around Iceland, where Atlantic Water inflow, Arctic waters, and local surface fluxes shape upper-ocean  
146 properties. Using a 29-year hydrographic time series, we investigate the variability of water-mass properties, mixed-layer  
147 depth (MLD), density, and thermohaline structure across seasonal and interannual timescales. We examine correlations  
148 with atmospheric circulation patterns such as the North Atlantic Oscillation (NAO) and, to complement the observations,  
149 use a 1D PWP model to simulate the mixed-layer response to local forcing, helping to identify the mechanisms driving  
150 MLD variability.

Deleted: At the regional scale, it is challenging to determine the extent to which changes in stratification and in water-mass properties are driven by natural or human-induced variability. Moreover, the relatively short observation records in most of the oceanic regions hinder the attribution of the observed changes to the driving mechanisms and forcings. In this study, by using a long time series of hydrographic observations around Iceland spanning 29 years, we aim at unraveling the different scales of variability of the water-mass properties, MLD, and stratification around Iceland. ...

Formatted: Font: Not Bold

Formatted: Font: Not Bold

Formatted: Font: Not Bold

Formatted: Font: Not Bold

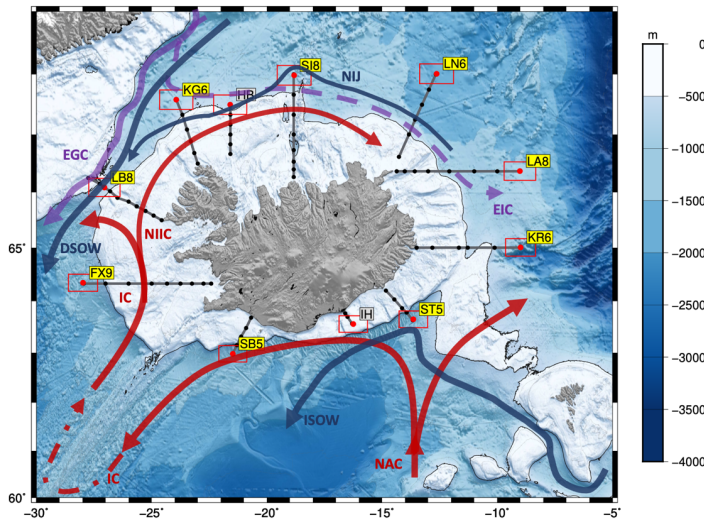
Deleted: ¶

151 **2 DATA AND METHODS**

152  
153 We use Conductivity-Temperature-Depth (CTD) data from the repeated hydrographic observational program of the  
154 Icelandic Marine and Freshwater Research Institute between 1990 and 2019. The oceanographic surveys took place  
155 quarterly, mainly in February, May, August, and November with little coverage during the intermediate months.  
156 Observations are made at standard repeated sections. The profiles are obtained with a Seabird 911plus CTD mounted on a  
157 rosette with Niskine bottles. The conductivity data are calibrated with salinity samples taken at the bottom of each station.  
158 All sensors underwent regular calibrations by the manufacturer.

159 In our analyses we considered only the deepest stations in each section (red dots in Fig. 1), including nearby stations  
160 within an area defined by 1° × 0.5° in longitude and latitude (red boxes). The selected stations are located outside of the  
161 Icelandic shelf (about 500 m depth). This criterion was chosen to avoid topographic effects, such as across shelf processes

185 on the stratification of the water column and to avoid MLDs limited by shallow bathymetry. Thus, the stations in gray, HB  
 186 and IH in Figure 1 were not considered as they fall on the shelf. For the sake of simplicity, stations will be named with the  
 187 acronym of the standard section, first two letters and the station number. The station full name (section and station number)  
 188 can be found in Table 1.



189  
 190 Figure 1: Map of the typical hydrographic sections collected by the Marine and Freshwater Research Institute around Iceland; the  
 191 black dots represent the nominal location of the standard stations from 1990-2019. The red dots are the stations used for this analysis  
 192 and the red boxes delimit the area within which all data were considered for this study. The grey bathymetric contours are spaced  
 193 every 100 m for the shallow water until the 500 m depth (thick black line) and then every 500 m. The hydrographic stations shown  
 194 in the yellow boxes corresponding to the standard sections: Faxaflói (FX9), Látrabjarg (LB8), Kögur (KG6), Hornbanki (HB),  
 195 Siglunes (SI8), Langanes NE (LN6), Langanes E (LA8), Krossanes (KR6), Stokksnes (ST5), Ingólfshöfði (IH) and Selvogsbanki  
 196 (SB5). The gray labeled IH and HB were not used in this analysis. The main surface and deep currents are also depicted on the map.

197 In this study we analyze the inter-annual variability and linear trends of the ML over a 29-year period as well as the  
 198 seasonal variability using the seasonal extremes (summer and winter), when there is more data coverage. From the CTD  
 199 stations we estimated the MLD using the density threshold method with a criterion of  $\sigma_\theta = 0.01 \text{ kg m}^{-3}$  (as, for instance,  
 200 in Piron et al., (2016) in the Irminger Sea) and a reference depth of 10 m. We chose this criterion instead of the usual  $0.03$   
 201  $\text{kg m}^{-3}$  (de Boyer Montégut, 2004) as the latter overestimated the MLD in more than 500 visually inspected profiles (not  
 202 shown). For comparison and robustness of our chosen method, we also estimated the MLD using other criteria (de Boyer  
 203 Montégut et al., 2004; Holte et al., 2017). We found the density threshold method appropriate for our region as it proves to  
 204 be effective even for cases where the variations of salinity and temperature were large. Those variations usually compensate  
 205 in density making this method more suitable. We have validated our method against previous work by Våge et al., 2018,  
 206 where a glider data was available, and the results were satisfactory. However, automatic detection methods have  
 207 limitations, as they may miss, for example, stacked mixed layers and other non-canonical representation MLs.

208 For each profile we computed the Brunt -Väisälä frequency ( $N^2$ ), defined as:

$$209 N^2 = g \frac{1}{\rho_0} \frac{\partial \sigma_\theta}{\partial z} \quad (1)$$

210 where g is the acceleration due to gravity,  $\rho_0$  is a reference density,  $\sigma_\theta$  is the potential density and z is depth.  $N^2$  can

Deleted: these

Deleted: ¶

Deleted: 8

Deleted:  $\int_\theta$

Deleted: =

Deleted: De Boyer Montegut

Deleted: c

Deleted: However, w

Deleted: shows

Deleted:

Formatted: English (CAN)

Deleted:  $\sigma$

Deleted:  $\theta$

Deleted: gravity

Deleted:  $\int_\theta$

225 be decomposed to show the relative contribution of salinity and temperature to the observed stratification as follows:

226  
227 
$$N^2 = N_T^2 + N_S^2, \quad (2)$$

228 where  $N_T^2$  and  $N_S^2$  are the components representing the stratification set by the temperature and salinity, respectively and  
229 are defined as:

230 
$$N_T^2 = g \left( \alpha \frac{\partial T}{\partial z} \right), \quad (3)$$

231  
232 
$$N_S^2 = g \left( \beta \frac{\partial S}{\partial z} \right), \quad (4)$$

233 where  $\alpha$  is the thermal expansion coefficient and  $\beta$  is the haline contraction coefficient at constant pressure. This  
234 decomposition has also been made to classify the oceans by their stratification contribution into  $\alpha$ -ocean,  $\beta$ -ocean, and  
235 transition zone, where in  $\alpha$ -oceans stratification is permanently dominated by temperature, in  $\beta$ -oceans by salinity and the  
236 transition regions are either intermittently or seasonally dominated by temperature or salinity (Carmack, 2007; Stewart and  
237 Haine, 2016). For the water column to be statically stable,  $N^2$  must be positive. However, the contributions may not be  
238 positive; when any of its components,  $N_T^2$  or  $N_S^2$  are negative, temperature or salinity respectively has a destabilizing effect  
239 on the resulting stratification that must be compensated by the other variable to maintain a stable water column. Small  
240 values of  $N^2$  indicate that the water column is weakly stratified which favors mixing due to winter convection and deeper  
241 MLD.

242 To investigate further, the driving mechanism of the MLD we used the Price-Weller-Pinkel (PWP), one-dimensional  
243 model (Price et al., 1986). The PWP model is a one-dimensional vertical model used to simulate the evolution of the ocean  
244 mixed layer in response to atmospheric forcing, including wind stress, heat fluxes, and freshwater fluxes. The model  
245 evolves vertical profiles of temperature, salinity, density, and horizontal velocity based on surface forcing and a set of  
246 physical stability criteria. The first criterion is convective overturning. If surface cooling increases the density such that  
247 the water column becomes gravitationally unstable (i.e., denser water overlies lighter water), the model applies vertical  
248 mixing until static stability is restored. The second criterion is based on the bulk Richardson number, which represents  
249 wind-driven mixing. The mixed layer deepens until the bulk Richardson number ( $R_{ib} = (g\Delta\rho h) / (\rho_0(\Delta U)^2)$ ) reaches or exceeds  
250 the critical values 0.6. The final criterion is the Gradient Richardson Number  $R_{ig} = N^2 / (\partial U / \partial z)^2$  which accounts for shear  
251 instability. When  $R_{ig} < 0.25$  local vertical mixing is applied. The PWP model is initialized with ERA-5 12-hour dataset of  
252 wind stress, heat, and freshwater fluxes (Hersbach et al., 2020) and the summer/winter averaged vertical profiles of  
253 temperature and salinity from the observations presented here (Fig. S1-S3). The 1D model allows to address the relative  
254 contributions from diurnal heating/cooling, freshwater fluxes, and wind mixing.

256 In addition, we broaden the impact of our findings by using the hydrographic database published in Brakstad (2023)  
257 that includes, in addition to the dataset from the Marine and Freshwater Research Institute of Iceland, other multiplatform  
258 observations like Argo floats or cruise data between 1950 and 2019. For this objective, a larger oceanic region is used and  
259 classified into  $\alpha$ -ocean and  $\beta$ -ocean using the spice frequency,  $K^2$ , (Carmack, 2007; Strehl et al., 2024), defined as:

260 
$$K^2 = N_T^2 - N_S^2. \quad (5)$$

261  $K^2$  is positive (negative) in  $\alpha$ -( $\beta$ -)oceans.

Deleted: more

Deleted: a

Formatted: Font: Not Italic

Formatted: Font: Not Italic

Deleted: see supplementary material

Deleted: would reveal the

Formatted: Font colour: Auto, English (CAN)

266

### 267 3 RESULTS

#### 268 3.1 Hydrographic properties around Iceland

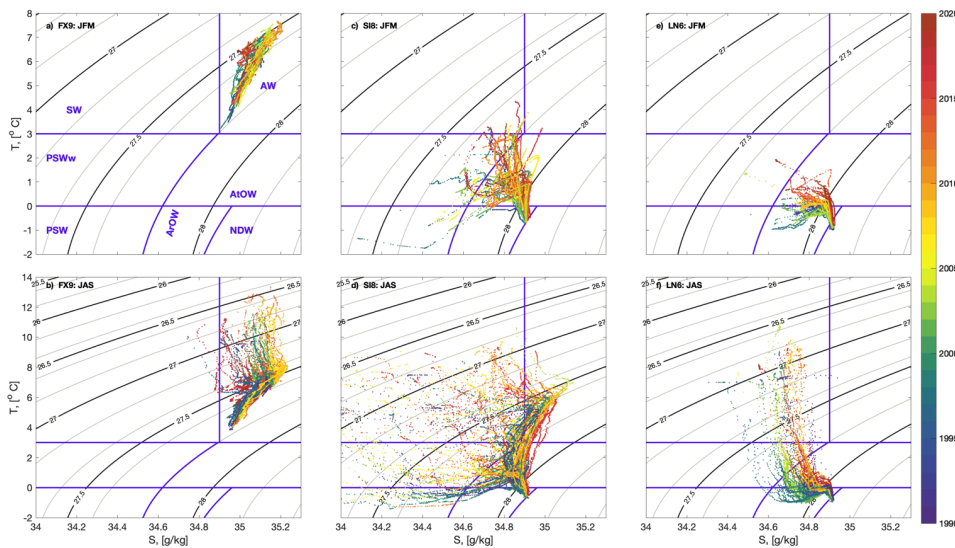
269 The hydrographic properties (potential temperature-salinity diagrams) around Iceland show important spatial, seasonal  
 270 and interannual variability are shown in Figure 2; the T/S properties differ widely between the three representative stations:  
 271 FX9, SI8 and LN6 for the west, north and northeast of Iceland. FX9, in the southwest of Iceland, is completely dominated  
 272 by Atlantic Water (AW; Fig. 2 a and b). At SI8, in the north, the dominating water masses in winter are of polar origin, i.e.,  
 273 warm Polar Surface Water (PSWw) in the upper layers, and Atlantic Overflow Water (AtOW) and Arctic Overflow Water  
 274 (ArOW) in the intermediate/bottom waters (Fig. 2c and d). The SI8 station also presents the largest variance of its  
 275 thermohaline characteristics. It is noteworthy that using fixed definitions of water masses may lead to biased estimates, as  
 276 these water masses have been steadily warming over the past two decades.  
 277 LN6, in the northeast, contains the coldest and densest waters on average (Fig. 2c and f).

Deleted: N

Deleted: dispersions

Deleted: N

278



279

280 **Figure 2: (Top row) Winter (JFM) and (bottom row) summer (JAS) T-S diagrams for three selected stations (a, b) FX9, (c, d) SI8**  
 281 **and (e, f) LN6, considered as representative for the south, north and northeast regions shown in Fig. 1. The T-S individual profiles**  
 282 **are color-coded by year. The main water masses as defined in Table 2, are labeled in panel (a).**

Deleted: S

Deleted: N

Deleted: N

Deleted: due to seasonal warming of the upper layers

283 The three stations have a clear seasonality. Overall, due to seasonal warming of the upper layers, the summer profiles  
 284 span a wider temperature range (Fig. 2b, d, f) than in winter (Fig. 2a, c, e). FX9 is notably warmer and saltier than the other  
 285 stations, especially in summer (Fig. 2a), when the minimum temperature in FX9 (nearly 4°C) is as high as the maximum  
 286 temperature in SI8 and 2 degrees higher than in LN6 (Fig. 2a, b, c). At SI8 a large change in density between seasons is  
 287 observed mainly driven by the contribution of AW, explained by offshore migration of the NIIC and the stronger inflow of  
 288 AW during the summer (Fig. 2c, and f) (Jónsson and Valdimarsson, 2012). While the widest seasonal amplitude in salinity  
 289 is observed at SI8, the largest seasonal amplitude in temperature is observed at LN6.

297 FX9 does not show a clear interannual pattern in summer but in winter the 2000's are strikingly saltier than the other  
298 years. In contrast, at SI8 and LN6 fresher and colder waters are observed in the 90's, they progressively warm and become  
299 saltier over time, and they reach their maximum temperature and salinity by 2015-2018. This decadal pattern is more  
300 evident in winter, but it is observed in both seasons.

### 301 3.2 Seasonality of Stratification and Mixed Layer Depth (MLD)

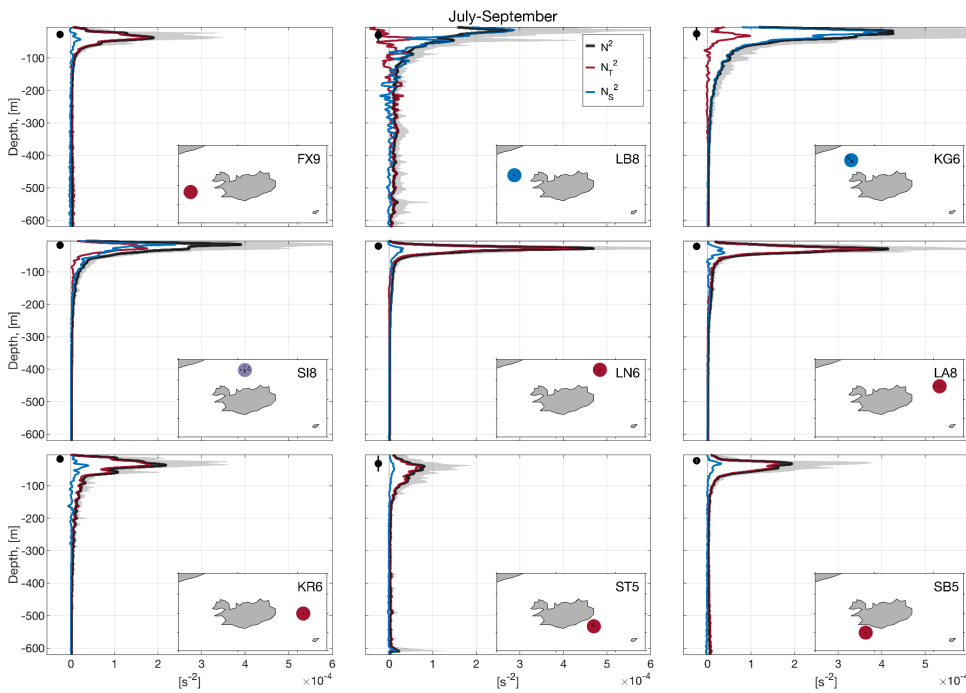
302 The spatial and temporal variability of the stratification around Iceland is remarkably large (Fig. 3 and Fig. 4), and the  
303 relative contribution of temperature and salinity shows a strong seasonal cycle. In summer, the MLD is relatively shallow,  
304 oscillating around 50 m with a small standard deviation (Fig. 3). In contrast, in winter the ML reaches depths greater than  
305 400 m in FX9, ST5 and SB5 with large standard deviations spanning a 100 m range (Fig. 4). The deepest average MLD is  
306 found in FX9 while the shallowest are KG6, SI8, LA8 and KR6.

307 In summer (Fig. 3), the upper-ocean stratification around Iceland (Fig. 3) is generally dominated by temperature, except  
308 for the three northwestern stations (namely LB8, KG6, SI8). LB8 exhibit the largest variability in both  $N_T^2$  and  $N_S^2$ , but is  
309 mainly dominated by salinity in the upper 200 m and by temperature below that depth. This transition station is located at  
310 the sill of Denmark Strait, a convergence zone for several currents (see Table 1 and Fig. 1) carrying water masses with  
311 contrasting T-S properties within the ML and the thermocline (Jónsson, 1999; Logemann et al., 2013; Casanova-Masjoan  
312 et al., 2020). In KG6, the fresh inflow from the EGC compensates for the cold temperature, and salinity largely dominates  
313 stratification. For SI8, we observe a mixed regime with almost equal contributions from both salinity and temperature to  
314 the total stratification, which suggests that this is also an area of transitional regime. For the stations: LN6, LA8 and KR6,  
315 despite the fact that stratification is mainly dominated by temperature, exhibit a small subsurface contribution of salinity  
316 just below the ML, likely due to the presence of fresh PSWw. The southern stations ST5 and SB5, have a minimal  
317 contribution to stratification from salinity, which may be associated with the numerous river discharges and the proximity  
318 to the continental shelf. The river discharge is the largest near SB5, likely explaining the summer subsurface contribution  
319 to salinity (Whitney, 2025).

Deleted: N

Deleted: s

Deleted: s



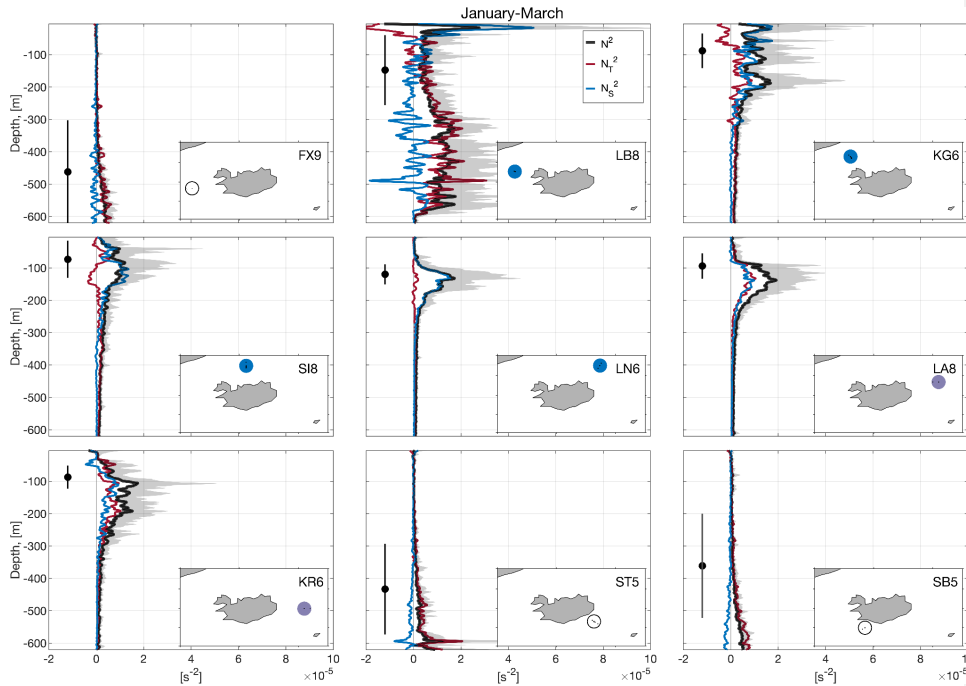
323  
 324 **Figure 3: Summer (JAS) average density stratification ( $N^2$ ) profiles for the selected stations; the average total stratification (black)**  
 325 **is decomposed into temperature (red) and salinity (blue) contributions, while the gray shaded band represents all the stratification**  
 326 **profiles. The black solid dot (left of the profiles) represents the average MLD with the error bar showing the standard deviation as**  
 327 **an indicator of the temporal variability. The maps in the lower corner show the location of the station within a circle color coded by**  
 328 **the dominating regime according to the contribution to stratification: red for temperature, blue for salinity, and purple for a mixed**  
 329 **regime.**

Deleted: salinity, and

330 The hydrographic conditions are very different for winter; the stratification is one order of magnitude lower, i.e.,  
 331 comparing Figure 3 and Figure 4. Also, the water temperature is much colder due to winter heat loss. Under these  
 332 conditions, the relative contribution of salinity to the total stratification stands out around Iceland except at the southern  
 333 stations (FX9, SB5, ST5), where the weakest winter stratification is observed. This southern region shows the deepest  
 334 MLD, between 350 and 700 m in the stations FX9, SB5 and ST5, while for the northern stations (KG6, SI8, LN6, LA8,  
 335 and KR6) the mean winter MLD is about 100 m. Similar to summer, station LB8, also shows high variability in winter  
 336 stratification, associated with the confluence of currents at the Denmark Strait.

337 The role of temperature or salinity in setting the stratification ( $\alpha$ - and  $\beta$ - ocean, see *e.g.*, Carmack, 2007) is linked to the  
 338 hydrographic characteristics (temperature and salinity) of the dominant water masses within each region. Based on this, we  
 339 can classify the waters around Iceland. The southern side is an  $\alpha$ -ocean as it receives the influence of warm and relatively  
 340 salty AW. Hence, the stratification is mainly temperature driven in both seasons (see FX9, ST5 and SB5 in Figures 3 and  
 341 4) and MLD gets deeper than 400 m in winter. The northwest of Iceland (LB8, KG6) is under the influence of the EGC  
 342 throughout the year bringing fresh PSW and PSWw into the area. Therefore, this area with winter MLDs of 100-150 m can  
 343 be considered a  $\beta$ -ocean, with heat fluxes equivalent to the southern region but with stronger and salinity dominated  
 344 stratification blocking the potential for deep convection, i.e., this region does not have a mechanism to lose surface  
 345 buoyancy seasonally in the salinity component. In contrast, the northeastern Icelandic area (SI8, LN6, LA8 and KR6) shifts

347 from  $\beta$  in winter to a mixed  $\alpha/\beta$  in summer. This is likely due to an offshore migration of the NIIC increasing the inflow of  
 348 AW (Jónsson and Valdimarsson, 2012; Casanova-Masjoan et al., 2020, their Figure 11). For instance, in winter, SI8 has a  
 349 PSW signature at the thermocline with salinity driving the stratification and a MLD of about 90 m ( $\beta$ -ocean), and in summer,  
 350 the NIIC brings warm AW to the upper layers of SI8 making the stratification similarly driven by temperature and salinity.  
 351 Overall, the north of Iceland exhibits the strongest summer stratification of the study area which results in very shallow  
 352 MLDs.



353 Figure 4: Same as Figure 3 but for winter (JFM). The white color circles shown in the maps of stations ST5, SB5, and FX9 indicate  
 354 very weak winter stratification with no significant contribution of salinity or temperature.  
 355

### 356 3.3 Interannual to decadal variability of the mixed layer properties

357 To investigate the interannual to decadal ML variability we focused on three reference stations, considered representative  
 358 of the  $\alpha$ -ocean (FX9, West), transition (SI8, north) and  $\beta$ -ocean (LB8, northwest) regimes around Iceland. FX9 dominated  
 359 by relatively warm and salty AW, SI8 as a transition area, and LB8 dominated by cold and fresh PSW. The three stations  
 360 show strong interannual variability.

361 In FX9, to the West of Iceland, there is a correlation ( $R=0.69$   $p$ -value $<0.01$ ) between mixed layer temperature (MLT)  
 362 and salinity (MLS) anomalies. Between 1990 and 1998 the mixed layer was the deepest, the coldest, and the second freshest  
 363 period, as shown in Figure 5a, and d (positive MLD anomalies correspond to deeper ML and negative ones correspond to  
 364 shallower ML). Around the period 2000-2014, there is an increase in MLT and MLS as the ML becomes moderately  
 365 shallower. The winter MLD is the shallowest, saltiest, and warmest in 2010 (Fig. 5a, and d), where the temperature  
 366 contribution seems to control this minimum. From 2015 to 2018 the ML returns to the cold and fresh conditions of the 90's  
 367 but the MLD is average. The observed variability of the ML and its temperature in FX9 exhibits correlation ( $R$ ) with the  
 368 North Atlantic Oscillation (NAO); for MLD, the best correlation was  $R=0.53$ ,  $p$ -value $<0.01$  at lag zero; for MLS  $R=-0.52$ ,

Formatted: Indent: Left: 0 cm, First line: 0 cm, Right: 0 cm, Space Before: 0 pt, After: 10 pt, Widow/Orphan control

Deleted: ¶

Deleted: N

Deleted: N

Deleted: er

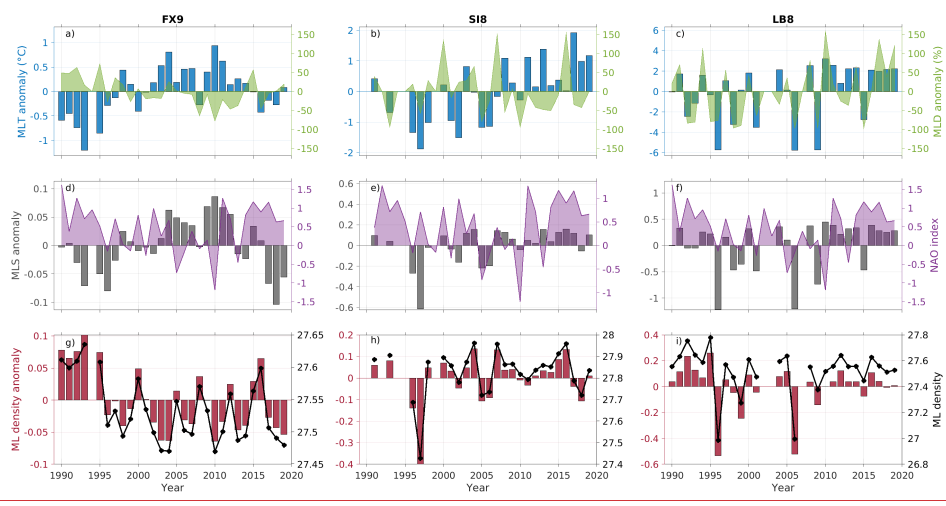
Deleted: certain

374 p-value<0.01 at lag -2 years (NAO leading), and for MLT  $R=-0.49$ , p-value<0.01 at lag -1 year (NAO leading (Fig. 5g, h).  
 375 However, we consider that a 2-year lag lacks a realistic physical explanation, thus, we prefer to not to consider this as a  
 376 reliable correlation. More qualitatively, positive NAO at the beginning and the end of the time series, corresponds with  
 377 deeper colder and fresher MLs, while negative NAO between 2000 and 2015 roughly corresponds with shallower, warmer,  
 378 and saltier MLs. As shown in Figure 2, FX9 contains only AW (Fig. 2a, d) likely advected from the south to the area by  
 379 the Gulf Stream and later the Irminger Current. Similar conditions have been observed in the Irminger Sea over the same  
 380 period, and they have been related to the NAO phase and its impact on the Subpolar gyre (Feucher et al., 2022). This  
 381 suggests that the FX region is largely influenced by the Atlantic climate and therefore it is partly impacted by the NAO  
 382 (Bersch, 2002).

383 At SI8, in the north of Iceland (Fig. 5b, e, h), the negative winter MLD anomalies are on the order of those at FX9 and  
 384 also exhibit strong interannual variability without an identifiable pattern. Strong positive MLD anomalies are observed in  
 385 particular years (e.g., 2000, 2007, and 2016) but they do not seem correlated with the MLT/MLS or with the NAO  
 386 variability. Interestingly, the MLT and MLS co-vary during the period 1990-2005, when the mixed layer is colder and  
 387 fresher, but this correlation weakens from 2005 to 2018, when the positive MLT anomalies increase while the MLS  
 388 anomalies, although positive, do not vary significantly.

389 In LB8 (northwest), the winter MLD has the largest variability as the station is located in the vicinity of the front between  
 390 NIIC and the EGC, which shapes the Polar and Atlantic conditions. Despite this large variability, a co-variance between  
 391 MLT and MLS anomalies seems to be correlated with the position of the front. Fresher and colder MLs are associated with  
 392 EGC influence and warmer/saltier MLs with the presence of NIIC (Fig. 5c, f, i). Generally, shallower MLs are also fresher  
 393 and colder, which agrees with a salinity-dominated stratification in the upper layer (Fig. 4b). Three particular years present  
 394 relatively deep, cold, and salty MLs: 1996, 2006 and 2014. The observed interannual variability in the ML and its properties,  
 395 while large, does not seem to be correlated with the NAO, except the last decade where the high state of the NAO is  
 396 consistent with the positive MLT and MLS, suggesting a larger presence of the NIIC at this station.

397



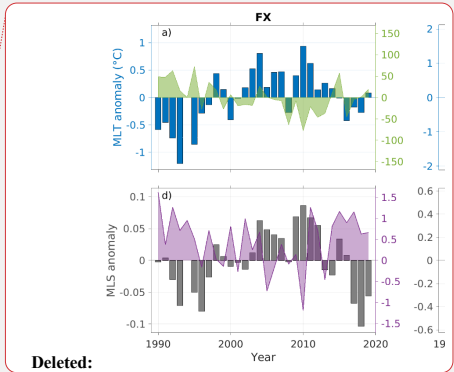
398  
399

Deleted: ,

Deleted: S

Deleted: N

Deleted: N



Deleted:



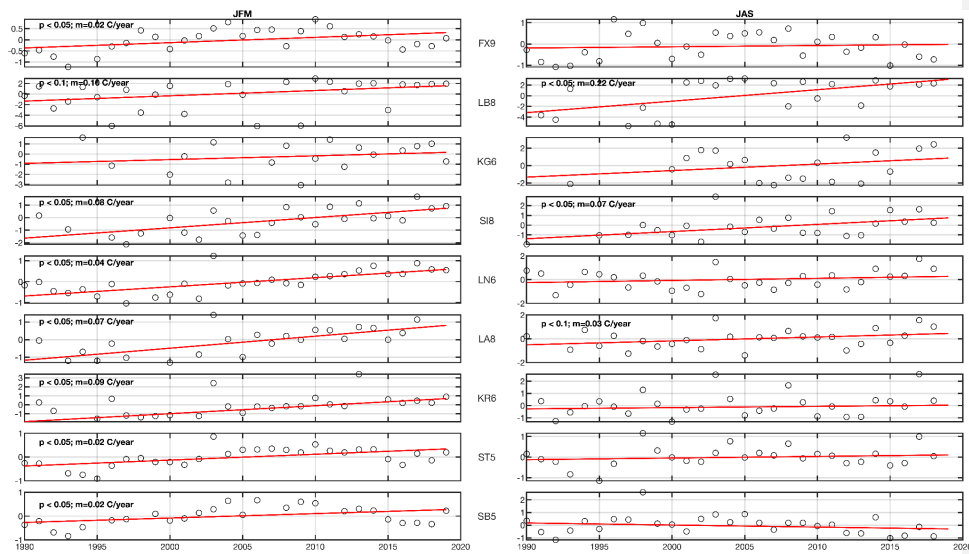


Figure 6: Mixed Layer Temperature (MLT) anomaly time series (left) winter (JFM) and (right) summer (JAS) for the 9 stations shown in Figures 3, 4. The anomalies show the p-values and the linear trends.

Similarly to Figure 6, in Figure 7 we compute the winter (JFM) density within the ML, which exhibits a statistically significant decrease for the stations in the south of Iceland (FX9, SBS, and ST5). The rest of the stations around Iceland do not show any significant changes. Remarkably, LN6, LA8, and SIB show no change in density even though they experience a significant increase in temperature.

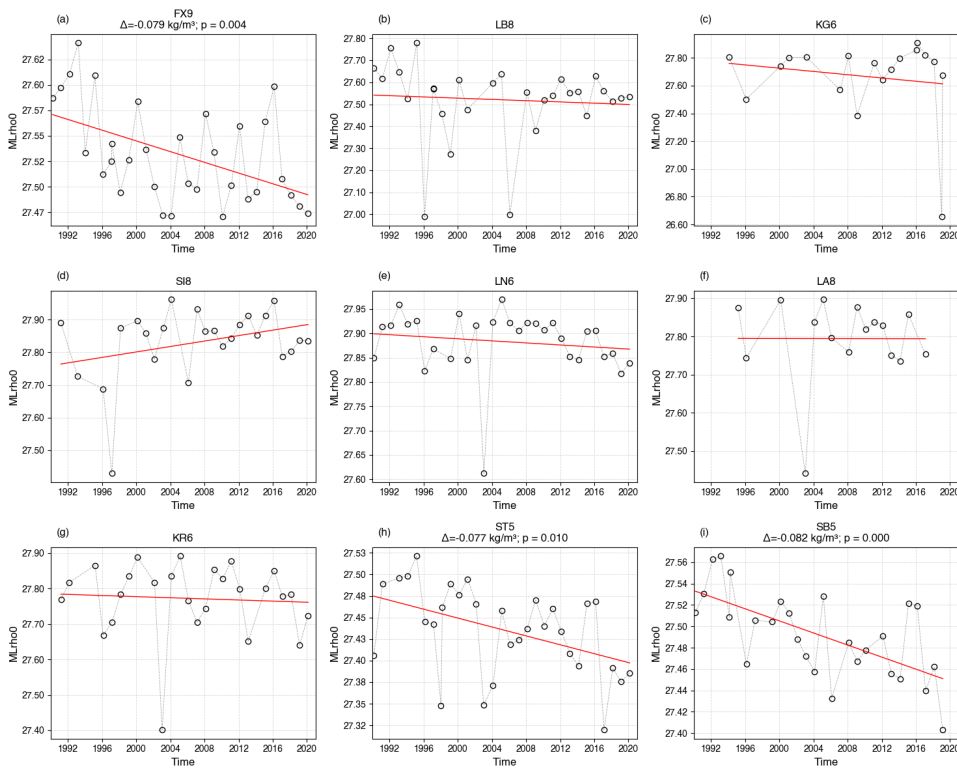


Figure 7: Mixed layer density (Mlrho) time series for the 9 representative stations only for winter (JFM). Stations FX9, ST5, and SB5 exhibit a statistically significant negative trend, with a total accumulated value of  $\Delta \sim -0.08 \text{ kg/m}^3$  over the 30 years of observations.

#### 4. MLD driving mechanisms from a 1D model

The summer stratification around Iceland in summer is roughly an order of magnitude higher than in winter, largely due to positive buoyancy forcing, resulting in shallower and more variable MLDs. Therefore, we study the atmospheric effect on these  $\alpha$ - and  $\beta$ -ocean regions by implementing the Price et al. (1986) one-dimensional model. The model is forced starting in the fall before the deep MLD develops. It is worth mentioning that the 1D model estimates the MLD from temperature-based profiles while the estimates from observations are density threshold based. The model results of the MLDs shown in Figure 8 are within the range of the observed average  $\pm$  standard deviations (thick black dots and lines in Fig. 8). For most stations a spring shoaling of the MLD is driven by reduced heat fluxes, while the MLD remains relatively deep due to the wind-stress. The choice of PWP model was made to support the idea that  $\beta$ - and transition oceans do not develop deep mixed layers, which is shown in Figure 8.

In the model, the stations embedded within the  $\alpha$ -ocean with AW (Fig. 8: FX9, SB5 and ST5) present the largest MLDs exceeding 300 m depth, which is consistent with the observations. In this  $\alpha$ -ocean region, the development of a deep ML is driven mainly by heat. However, within these stations, the wind-stress steadily contributes to the development of the ML. During the summer, shoaling of the mixed layer is likely influenced by the changes of both heat and freshwater fluxes, with

Formatted: Left

Deleted: and hence summer

Deleted: are very shallow and with higher variability

Formatted: Font: Not Italic

Formatted: Font: Not Italic

Formatted: Font: Not Italic

Formatted: Font: Not Italic

Formatted: Font: Not Italic

Formatted: Font: Not Italic

Formatted: Font: Not Italic

Formatted: Font: Not Italic

Formatted: Font: Not Italic

Deleted: Therefore, we only use the winter season to study the atmospheric effect on these  $\alpha$ - and  $\beta$ -ocean regions by using the Price et al. (1986) one-dimensional model. It is worth mentioning that the 1D model estimates the MLD from temperature-based profiles while the estimates from observations are density threshold based. The MLDs shown in Figure 7 are within the range of the observed average  $\pm$  standard deviations (black dots and lines in Figure 7). For all stations a spring shoaling of the MLD is driven by heat flux, while the MLD remains relatively deep due to the wind-stress. The choice of PWP model was made to support the idea that  $\beta$ - and transition oceans do not develop deep mixed layers, which is shown in Figure 7.

Formatted: Font: Not Italic

Formatted: Font: Not Italic

Deleted: in

Deleted:

Deleted: fluxes (Fig. 7 h and i), which also holds for FX9.

Deleted: (Fig. 7a, h and i).

their effects on the MLD partially offset by wind stress (Fig. 8: FX9, SB5 and ST5).

The station LB8, despite being in Denmark Strait and presenting a large contribution of PSWw and PSW in the upper layers (driving a  $\beta$ -ocean stratification), shows that the development of MLDs can be influenced by both, heat flux and/or wind stress (Fig. 8: LB8). However, the contribution of wind-stress and freshwater cannot lead to MLDs deeper than 100m (Fig. S4:LB8). Beneath the PSW and PSWw at LB8 we find AtOW. Hence as the wind-stress develops, the MLD evolution erodes the PSWw strata reaching the AtOW layer, allowing reduced heat fluxes to contribute to the MLD development. This erosion is not visible on the stations embedded within the EIC.

Wind stress becomes the leading forcing mechanism northeast of LB8 at stations KG6, and S18, coinciding with the shift from  $\alpha$ - to  $\beta$ -ocean stratification (Fig. 8). This region has a lower convective potential than regions with pure AW and therefore does not produce large MLDs (Fig. 4 and 8). The MLD there results from roughly equal contributions of convection and wind-driven mixing. At these stations, the best performance of the PWP model is obtained when both heat flux and wind-stress are included (Fig. S4). Notably, the summer MLD remains shallow and roughly with the same order of magnitude across all stations around Iceland (Fig. 8 and S4).

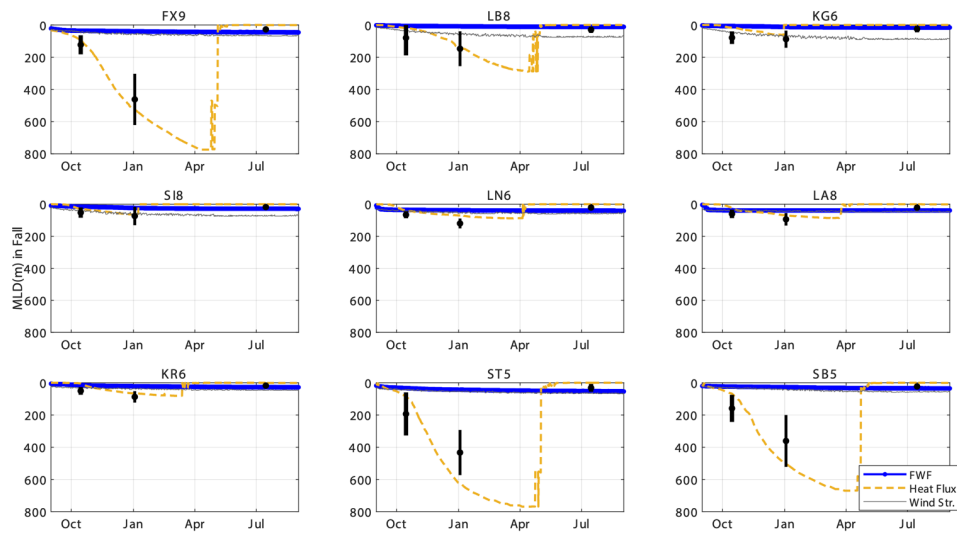


Figure 8: MLD driving mechanism decomposition estimated from the PWP 1-D model (Price et al. 1986) for each of the studied stations. Different MLD evolutions are shown for outputs forced with freshwater fluxes (blue), heat fluxes (red), and wind-stress (green). Black dots represent the averaged winter and summer MLD with their standard deviations.

### 5. Stratification around Iceland

To complement the understanding of the stratification of the Arctic and Subarctic waters around Iceland, their connection with water masses, currents, and their variability, we used the spiciness frequency averaged in the first 200 m, estimated following the methods described in Strehl et al. (2024) implementing Equation (5). For this analysis we used the hydrographic dataset in Brakstad et al (2023). The spiciness distributions shown in Figure 9 reveal that temperature dominates on the southern side of Iceland, marked by an  $\alpha$ -ocean regime, while salinity dominates the northern side,

Deleted: (Fig. 7a, h and i).

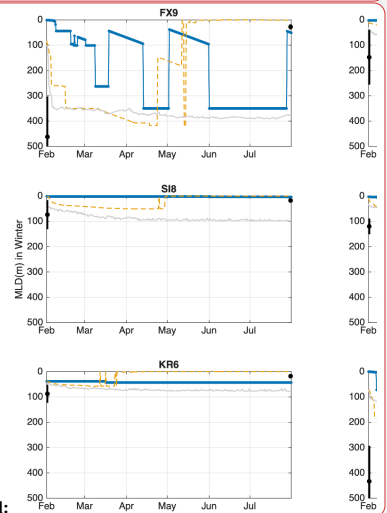
Formatted: Left

Deleted: . 7b

Formatted

Formatted

Deleted: leads to a slightly deeper MLD than the heat fluxes (Fig. 7b). Wind stress becomes the lead forcing mechanism northeast of LB8 (KG6, S18), coinciding with the shift from  $\alpha$ - to  $\beta$ -ocean stratification (Fig. 7b, c and d). This region represented by LB8 station does not have a large convection potential compared to those with pure AW and hence do not produce large MLDs (Fig. 4) and the MLD is a result of convection wind-mixing in roughly equal parts. At LN6, LA8 and KR6 before spring, wind-stress and heat fluxes contribute similarly to the development of the MLD; those stations are at the core of the EIC, which contains PSWw in the upper layers and AtOW beneath. Hence the wind-stress and heat fluxes are the driving mechanisms acting on the water column (Fig. 7e and f). As the wind-stress develops, the MLD evolution erodes the PSWw strata reaching the AtOW layer, allowing the heat fluxes to lead the MLD development.



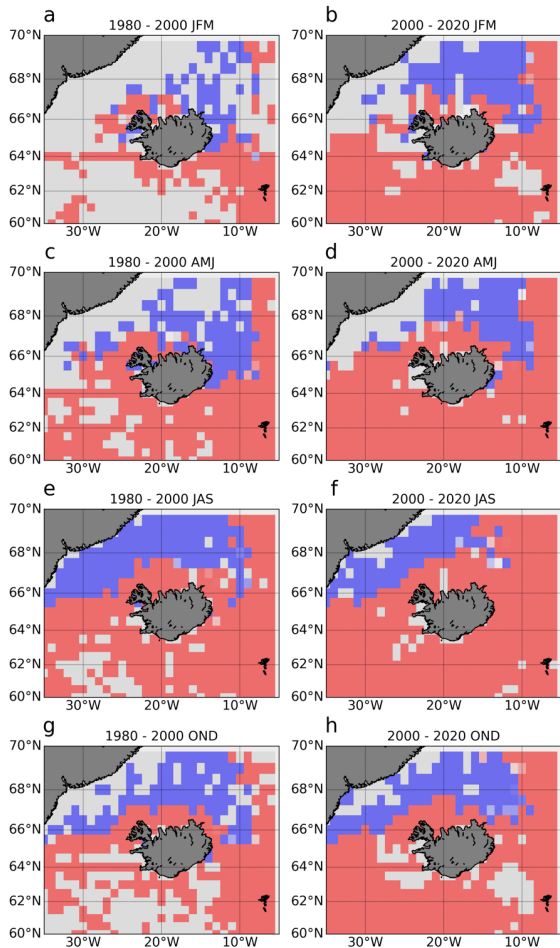
Deleted:

Deleted: 7

Deleted: 8... clearly

558 associated with  $\beta$ -ocean. These areas largely correspond with the distribution of AW versus PSW/PSWw (See Fig. 2 for  
 559 T-S definitions).

Deleted: s a southern (northern) side where the temperature (salinity) dominates the spiciness and hence marking clear  
 Deleted:  $\alpha$ -ocean regimes, while the northern part has salinity dominated regions associated with  $\beta$ -ocean.



560  
 561 **Figure 9:** Mean upper 200m spice frequency for the region of study showing the  $\alpha$ -ocean (red) and  $\beta$ -ocean (blue) regions for the  
 562 periods of 1980-2000 and 2000-2020 and the four main seasons JFM (a,b), AMJ (c,d), JAS (e,f) and OND (g,h). The Brakstad et al  
 563 (2023) hydrographic dataset is used for this calculation.

Deleted: 8  
 Deleted: frequency for

564 The seasonal distribution of spice frequency north of Iceland agrees with the seasonal behavior of the NIIC described in  
 565 Casanova-Masjoan et al. (2020) where the NIIC surface extension in winter and spring remains constrained to the northwestern  
 566 side of Iceland due to the cold southeast surface imprint of the EIC. Then in summer, the NIIC expands northeastward, reaching  
 567 all the way to the eastern side of Iceland and the northernmost station at the SI transect and constraining the polar water  
 568 between the northern end of the Kolbeinsey Ridge and the Greenland shelf. Then in fall the NIIC northern extension narrows  
 569 but is still able to surround Iceland. It is noteworthy that a clear increase in coverage of the  $\alpha$ -ocean, mainly in summer, is  
 570 observed by comparing the 1980-200 average and the 2000-2010 average.

577 6. DISCUSSION AND CONCLUSIONS

578 In this study, we discussed the seasonal and interannual variability of the mixed layer characteristics and the stratification  
579 regimes around Iceland by using a long time series of CTD data. Based on our results, we propose the regionalization of  
580 the waters around Iceland into three dynamical regions  $\alpha$ -ocean,  $\beta$ -ocean, and transition-ocean.

581 The southwestern region is dominated by AW both in winter and summer. Within this region, the winter MLD  
582 is the deepest and most variable of the whole study area, with ML's occupied by AW over the whole sampling period.  
583 This region is influenced by the dynamics of the Irminger Sea and the Subpolar gyre and has favorable conditions ( $\alpha$   
584 -ocean) for winter deep convection driven by heat fluxes to develop deep mixed layers, which agrees with previous  
585 studies (Carmack, 2007; Våge et al., 2008; Piron et al., 2016; Stewart and Haine, 2016; Petit et al., 2020). In the  
586 southern region, the ML salinity anomaly was negative over the last 5 years, which is consistent with previous  
587 numerical models and Argo observations showing a freshening trend of the North Atlantic (Tesdal et al., 2018;  
588 Holliday et al., 2020; Liu et al., 2020). However, since the south of Iceland is an  $\alpha$ -ocean, these recent changes have  
589 not yet reached or affected the MLD.

590 The northwestern region, which includes the Denmark Strait, is a medley of all the water masses described in this study.  
591 In this region there is a confluence of Greenland shelf and slope waters and Iceland Sea origin waters (Harden et al., 2016;  
592 Foukal et al., 2020). This includes the NIIC generating an important variability in the water properties due to complex  
593 interactions of the regional currents (Lin et al. 2020, Mastropole et al. 2017). The MLD variability over time at the KG6  
594 and LB8 stations is moderate (<100m), except for the years 2000, 2007 and 2016 when the ML was anomalously deep. In  
595 this region, the stratification is notably year-round dominated by salinity ( $\beta$ -ocean), which is explained by the strong Polar  
596 influence of cold and fresh waters transported by the EGC. A broader look into the northwestern side of the basin reveals  
597 that this area can be divided at the center of the Denmark Strait into an  $\alpha$ -ocean near the Icelandic shelf where the NIIC  
598 flows and a  $\beta$ -ocean as we progress towards Greenland (where the LB8 and KG6 stations are located). Near the Icelandic  
599 shelf, MLDs are driven mainly by wind-stress, with a secondary contribution of heat fluxes. The T-S properties as well as  
600 the MLT anomalies in the northwest region near the Icelandic shelf show that the NIIC waters there are getting warmer and  
601 saltier. This agrees with previous studies showing the transformation of the NIIC also accompanied by an increase in its  
602 transport with time (Casanova-Masjoan et al., 2020). Even if the  $\alpha$ -ocean area is warming, it is not expanding  
603 northwestward. Hence, the EGC is acting as a barrier bringing PSW in the area and maintaining the  $\beta$ -ocean state on the  
604 northwesternmost side of the Strait. This  $\beta$ -ocean, where the MLD is shallow all year round has dynamical implications as  
605 the strong shallow stratification inhibits baroclinic instability and eddy generation (de Marez et al., 2025).

606 Northeast of Iceland, the ML exhibits intrusions of SW in the winter, while AW is present during the summer. In this  
607 region, the stratification changes from  $\beta$ - to  $\alpha$ -ocean seasonally. The Kolbeinsey Ridge acts as a barrier where we find the  
608 eastward penetration of the EIC bringing fresh waters (PSWw) from the East Greenland Current (Macrander et al., 2014;  
609 Casanova-Masjoan et al., 2020). In summer, the NIIC expands northeastward, bringing AW into the area and changing the  
610 stratification regime to  $\alpha$ . Hence, the mixed layer waters show important seasonal variability. They range from maximum  
611 temperature below 2 °C in winter to over 10 °C in summer. This is also the only region where a significant warming decadal  
612 trend emerges over the interannual variability and progressively results in a stronger  $\alpha$ -ocean. This agrees with the AW  
613 warming observed in Casanova-Masjoan et al. (2020) and with the northward progression of AW named as 'Atlantification'  
614 described by Polyakov et al. (2017). This shift to  $\alpha$ -ocean or 'Atlantification' may lead to deeper ML's (Moore et al., 2015;  
615 Våge et al., 2022), and the associated deeper convection may increase the potential of this area to contribute to the dense  
616 flow carried by the NIJ (Semper et al. 2019).

Deleted: S

Deleted: S

Formatted: English (CAN)

619 The regionalization proposed in this work, based on hydrographic properties, matches the recently proposed distribution  
620 of primary production around Iceland (Richardson and Bendtsen, 2021; Cerfonteyn et al., 2023), supporting the importance  
621 of MLD properties for the primary production (Ólafsson, 2003). The induced alterations on primary production can lead to  
622 ecosystem changes. For example, Iceland has witnessed a rapid increase in the population of mackerel, a relatively warm-  
623 water fish, since 2006 (Astthorsson et al., 2012; Campana et al., 2020) starting from the ~~s~~southeast towards the north and  
624 recently they have been reported almost all around the country. This migration is consistent with our observations of both,  
625 the increase in surface temperatures, *i.e.*, northward shift of warmer isotherms over the Iceland Faroe Ridge (de Marez et  
626 al., 2025), and the increase of temperatures within the ML in the same regions over the last decade, which may establish  
627 new pathways for entire ecosystems.

Deleted: S

628 The long time series investigated here revealed important interannual oscillations of the ML properties. Four main  
629 features are to be highlighted: (i) We do not observe any linear trend in the MLD, which is rather subjected to strong  
630 interannual variability (ii) Except for the southern stations, influenced by the subpolar gyre, the interannual variability was  
631 not correlated with the NAO. For example, FX9 shows a significant negative of MLT with the NAO ( $R=-0.41$  and  $p\text{-value}$   
632  $< 0.03$ ). (iii) ~~The southern stations, FX9, SB5, and ST5, within the  $\alpha$ -ocean region, show a clear decrease in ML density,~~  
633 ~~with statistically significant values and accounting for a total decrease during the 29-year period of  $-0.08 \text{ kg/m}^3$ .~~ (iv) The  
634 linear fit indicates significant (at 95%) warming trends in the MLT of most of the stations in winter, with the maximum  
635 trend of  $0.08 \text{ }^\circ\text{C/year}$  at S18 resulting in approximately  $2.2 \text{ }^\circ\text{C}$ . This agrees with previous studies (Sarfanov, 2009) showing  
636 that the northern part of the North Atlantic (~~south of Iceland~~) is strongly dominated by atmospheric interannual to decadal  
637 variability, particularly, where AW is present. The exception here is the ~~n~~ortheastern region of Iceland where we observe  
638 a clear warming trend of the ML (2010-2020). (v) ~~We observe an ‘Atlantification’ expressed as a northeastward progression~~  
639 ~~of the  $\alpha$ -ocean state. This progression will highlight the role of the northeastern area of Iceland as a convective zone where~~  
640 ~~deep water could be formed and contribute to the NIJ.~~

Deleted: ii

Formatted: Superscript

Deleted: S

Deleted: N

Deleted: i

## 641 AUTHOR CONTRIBUTIONS

642 Conceptualization, ARA, MDPH and EP; methodology, ARA, EP and MDPH; software, ARA and AP; formal analysis,  
643 ARA, EP, TM, CdM and MDPH; investigation, ARA, EP and MDPH, AM; data acquisition, SRÓ and AM; data curation,  
644 SRÓ and AM; writing—original draft preparation, ARA, EP and MDPH; writing—review and editing, SRÓ, AM and SJ,  
645 TM; visualization, ARA and EP; project administration, SRÓ; funding acquisition, ARA and SRÓ. All authors have read  
646 and agreed to the published version of the manuscript.

## 647 FUNDING

648 ARA ~~and CdM~~ have been supported by HM Queen Margrethe II's and Vigdís Finnbogadóttir's Interdisciplinary  
649 Research Centre on Ocean, Climate and Society (ROCS) under grant no. 158-4223. Support for this work was also  
650 provided by the European Union's Horizon 2020 research and innovation programme under grant no. 727852, Blue-  
651 Action project (AM and SJ). This work has been supported by the FAR-DWO (PID2020-114322RBI00) project from the  
652 Spanish Ministry of Research.

Deleted: s

## 653 ACKNOWLEDGMENTS

654 We are grateful for the invaluable cooperation we have had with the crews of the Icelandic research vessels Bjarni  
655 Sæmundsson and Árni Friðriksson and to the many people at the Marine Research Institute that have contributed to the

662 hydrographic observations over the years. ARA and MDPH would like to dedicate this paper to the memory of Maria  
663 Casanova-Masjoan.  
664

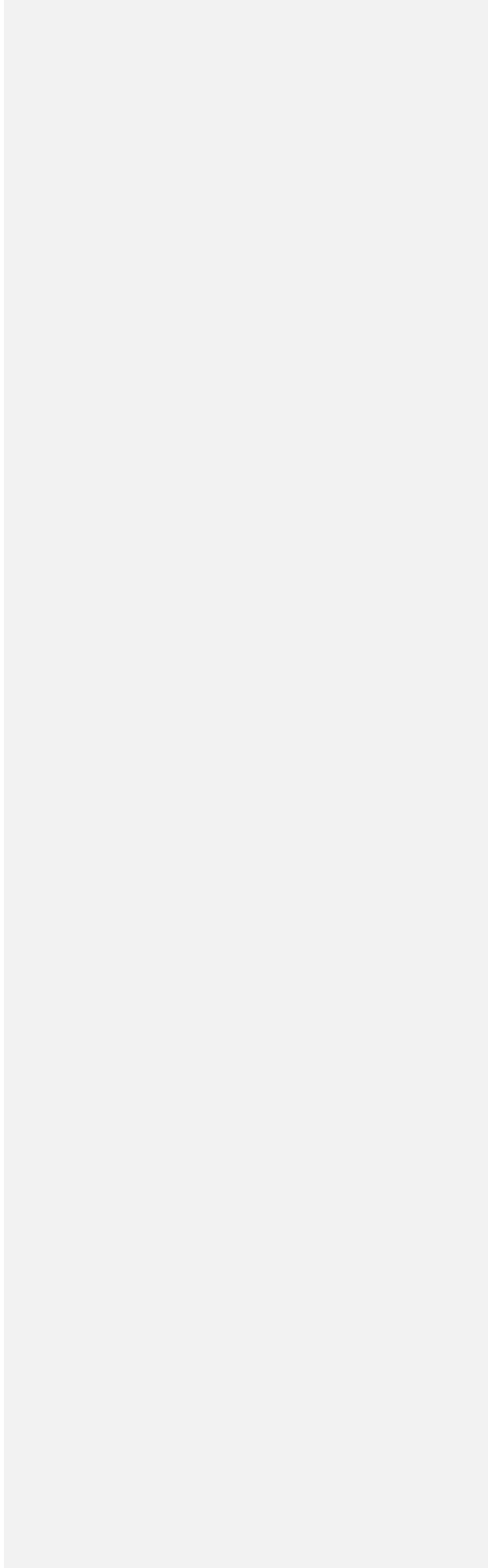


**Table 2.** Characteristics for the representative stations for each typical surveyed section. The representative ocean currents at each section are also shown: North Icelandic Irminger Current (NIIC), Irminger Current (IC), East Greenland Current (EGC), North Icelandic Jet (NIJ), East Icelandic Current (EIC), and North Atlantic Current. (NAC). The corresponding stratification regimes are listed for summer and winter for each station.

Station	Depth, [m]	Lon	Lat	Oceanic region	Significant currents	Stratification regime
Faxaflói (FX9)	1010	-27.98	64.35	Subpolar North Atlantic	IC	Alpha-ocean (summer) Weakly stratified (winter)
Látrabjarg (LB8)	658	-27.050	66.083	Denmark Strait	NIIC, EGC, DSO	Beta-ocean (all year round)
Kögur (KG6)	980	-23.933	67.583	Western Iceland Sea	EGC, DSO	Beta-ocean (all year round)
Síglunes (SI8)	1023	-18.83	68.00	Kolbeinsey Ridge	NIIC, EGC, EIC, NIJ	Transition (summer) Beta-ocean (winter)
Langanes NE (LN6)	1850	-12.66	68.00	Iceland Sea	EIC	Alpha-ocean (summer) Beta-ocean (winter)
Langanes E (LA8)	1251	-9.00	66.37	Iceland Sea	EIC	Alpha-ocean (summer) Transition (winter)
Krossanes (KR6)	1419	-9.00	65.00	Iceland Sea/ North Atlantic	EIC, NAC	Alpha-ocean (summer) Transition (winter)
Stokksnes (ST5)	1153	-13.66	63.66	North Atlantic	NAC	Alpha-ocean (summer) Weakly stratified (winter)
Selvogsbanki (SB5)	1006	-21.48	62.98	North Atlantic	IC	Alpha-ocean (summer) Weakly stratified (winter)

**Table 3.** Main water masses definitions for the region of study (Rudels et al., 2005; Våge et al., 2011)

Water mass	Potential Temperature ( $\theta$ )	Salinity	Potential density ( $\sigma_\theta$ , $\text{kg m}^{-3}$ )
Surface Water (SW)	$> 3^\circ\text{C}$	-	$\sigma_\theta < 27.70$
Warm Polar Surface Water (PSW <sub>w</sub> )	$0^\circ\text{C} \leq \theta < 3^\circ\text{C}$	-	$\sigma_\theta < 27$
Polar Surface Water (PSW)	$< 0^\circ\text{C}$ ,	-	$\sigma_\theta < 27.70$

Atlantic Water(AW)	$> 3^{\circ}C$	$> 34.9$	-
Atlantic-origin Overflow Water (AtOW)	$0^{\circ}C \leq \theta < 3^{\circ}C$	-	$\sigma_0 \geq 27.8,$ $\sigma_{0.5} < 30.44$
Polar intermediate Water (PIW)	$0^{\circ}C$	$\leq 34.676$	$\sigma_0 > 27.70,$
Arctic-origin Overflow Water (ArOW)	$< 0^{\circ}C$	-	$\sigma_0 > 27.8,$ $\sigma_{0.5} < 30.44$
Nordic Seas Deep Water (NDW)	$< 0^{\circ}C$	-	$\sigma_{0.5} \geq 30.44$

688  
689  
690  
691  
692  
693  
694  
695  
696  
697  
698  
699  
700  
701  
702  
703  
704  
705  
706  
707  
708

709

710

711 **References**

712 Astthorsson, O. S., Valdimarsson, H., Gudmundsdottir, A., and Oskarsson, G. J.: Climate-related variations in the  
713 occurrence and distribution of mackerel (*Scomber scombrus*) in Icelandic waters, *ICES J. Mar. Sci.*, 69, 1289–1297, 2012.

714 Athanase, M., Provost, C., Perez-Hernández, M. D., Sennechael, N., Bertosio, C., Artana, C., et al.: Atlantic water  
715 modification north of Svalbard in the Mercator physical system from 2007 to 2020, *J. Geophys. Res.: Oceans*, 125,  
716 e2020JC016463, <https://doi.org/10.1029/2020JC016463>, 2020.

717 Bachman, S. D., Taylor, J., Adams, K., and Hosegood, P.: Mesoscale and submesoscale effects on mixed layer depth in  
718 the Southern Ocean, *J. Phys. Oceanogr.*, 47, 2173–2188, 2017.

719 Bindoff, N. L., Cheung, W. W., Kairo, J. G., Aristegui, J., Guinder, V. A., Hallberg, R., et al.: Changing ocean, marine  
720 ecosystems, and dependent communities, *IPCC Special Report on the Ocean and Cryosphere in a Changing Climate*, 477–  
721 587, 2019.

722 Brakstad, A.: *Hydrographic and Geochemical Observations in the Nordic Seas Between 1950 and 2019*, University of  
723 Bergen, 2023b.

724 Bersch, M.: North Atlantic Oscillation–induced changes of the upper layer circulation in the northern North Atlantic Ocean,  
725 *J. Geophys. Res.*, 107(C10), 3156, <https://doi.org/10.1029/2001JC000901>, 2002.

726 Campana, S. E., Stefansdottir, R. B., Jakobsdottir, K., and Solmundsson, J.: Shifting fish distributions in warming sub-  
727 Arctic oceans, *Sci. Rep.*, 10, 1–14, 2020.

728 Carmack, E. C.: The alpha/beta ocean distinction: A perspective on freshwater fluxes, convection, nutrients and  
729 productivity in high-latitude seas, *Deep Sea Res. Part II: Top. Stud. Oceanogr.*, 54, 2578–2598, 2007.

730 Carton, J. A., Grodsky, S. A., and Liu, H.: Variability of the oceanic mixed layer, 1960–2004, *J. Climate*, 21, 1029–1047,  
731 2008.

732 Casanova-Masjoan, M., Perez-Hernández, M. D., Pickart, R. S., Valdimarsson, H., Ólafsdóttir, S., Macrander, A., et al.:  
733 Along-stream, seasonal, and interannual variability of the North Icelandic Irminger Current and East Icelandic Current  
734 around Iceland, *J. Geophys. Res.: Oceans*, 125, e2020JC016283, <https://doi.org/10.1029/2020JC016283>, 2020.

735 Cerfonteyn, M., Groben, R., Vaulot, D., et al.: The distribution and diversity of eukaryotic phytoplankton in the Icelandic  
736 marine environment, *Sci. Rep.*, 13, 8519, <https://doi.org/10.1038/s41598-023-35516-w>, 2023.

737 Dai, A., Luo, D., Song, M., and Liu, J.: Arctic amplification is caused by sea-ice loss under increasing CO<sub>2</sub>, *Nat. Commun.*,  
738 10, 1–13, 2019.

739 de Boyer Montégut, C., Madec, G., Fischer, A. S., Lazar, A., and Iudicone, D.: Mixed layer depth over the global ocean:  
740 An examination of profile data and a profile-based climatology, *J. Geophys. Res.: Oceans*, 109,  
741 <https://doi.org/10.1029/2004JC002378>, 2004.

742 de Marez, C., Ruiz-Angulo, A., & Gula, J. Mesoscale induced vertical fluxes over the Iceland-Faroe ridge. *Geophysical*  
743 *Research Letters*, 52(13), 2025.

744 [de Marez, Charly, Clara R. Vives, Esther Portela, and Angel Ruiz-Angulo. Mesoscale ocean processes: The critical role](#)  
745 [of stratification in the Icelandic region. \*Journal of Geophysical Research: Oceans\* 130, no. 6 \(2025\).](#)

746 Feucher, C., Portela, E., Kolodziejczyk, N., & Thierry, V. Subpolar gyre decadal variability explains the recent

Deleted: e

Formatted: Spanish

Formatted: English (CAN)

748 oxygenation in the Irminger Sea. *Communications Earth & Environment*, 3(1), 279, 2022.

749 Foukal, N. P., Gelderloos, R., and Pickart, R. S.: A continuous pathway for fresh water along the east Greenland shelf, *Sci.*  
750 *Adv.*, 6, eabc4254, 2020.

751 [Fox-Kemper, B., H.T. Hewitt, C. Xiao, G. Aðalgeirsdóttir, S.S. Drijfhout, T.L. Edwards, N.R. Golledge, M. Hemer, R.E.](#)  
752 [Kopp, G. Krinner, A. Mix, D. Notz, S. Nowicki, I.S. Nurhati, L. Ruiz, J.-B. Sallée, A.B.A. Slangen, and Y. Yu, 2021:](#)  
753 [Ocean, Cryosphere and Sea Level Change. In \*Climate Change 2021: The Physical Science Basis. Contribution of Working\*](#)  
754 [Group I to the Sixth Assessment Report of the Intergovernmental Panel on Climate Change \[Masson-Delmotte, V., P. Zhai,](#)  
755 [A. Pirani, S.L. Connors, C. Péan, S. Berger, N. Caud, Y. Chen, L. Goldfarb, M.I. Gomis, M. Huang, K. Leitzell, E. Lonnoy,](#)  
756 [J.B.R. Matthews, T.K. Maycock, T. Waterfield, O. Yelekçi, R. Yu, and B. Zhou \(eds.\)\]. Cambridge University Press,](#)  
757 [Cambridge, United Kingdom and New York, NY, USA, pp. 1211–1362, doi: 10.1017/9781009157896.011.](#)

758 [Gjelstrup CVB, Sejr MK, de Steur L, Christiansen JS, Granskog MA, Koch BP, Møller EF, Winding MHS, Stedmon CA.](#)  
759 [2022. Vertical redistribution of principle water masses on the northeast Greenland Shelf. \*Nature Communications\* 13:](#)  
760 [doi:10.1038/s41467-022-35413-z.](#)

761 Hafrannsóknastofnun: Makrill *Scomber scombrus* Stofnmatskýrslur (stock assessment report), Hafrannsóknastofnun,  
762 2024, [https://www.hafogvatn.is/static/extras/images/mackerel\\_2024\\_techreport\\_is.html](https://www.hafogvatn.is/static/extras/images/mackerel_2024_techreport_is.html).

763 Hansen, B., and Østerhus, S.: North Atlantic–Nordic Seas exchanges, *Prog. Oceanogr.*, 45, 109–208, 2000.

764 Harden, B., Renfrew, I., and Petersen, G.: Meteorological buoy observations from the central Iceland Sea, *J. Geophys.*  
765 *Res.-Atmos.*, 120, 3199–3208, 2015.

766 Harden, B. E., Pickart, R. S., Valdimarsson, H., Vage, K., de Steur, L., Richards, C., et al.: Upstream sources of the  
767 Denmark Strait overflow: Observations from a high-resolution mooring array, *Deep-Sea Res. Pt. I*, 112, 94–112, 2016.

768 Hátún, H., and Chafik, L.: On the recent ambiguity of the North Atlantic Subpolar Gyre Index, *J. Geophys. Res.-Oceans*,  
769 123, 5072–5076, 2018.

770 Hátún, H., Chafik, L., and Larsen, K. M. H.: The Norwegian Sea Gyre – a regulator of Iceland-Scotland Ridge exchanges,  
771 *Front. Mar. Sci.*, 8, 1001, 2021.

772 Havik, L., Pickart, R. S., Våge, K., Torres, D. J., Thurnherr, A., Beszczynska-Möller, A., et al.: Evolution of the East  
773 Greenland Current from Fram Strait to Denmark Strait: Synoptic measurements from summer 2012, *J. Geophys. Res.-*  
774 *Oceans*, 122, 1974–1994, 2017.

775 Hersbach, H., Bell, B., Berrisford, P., et al.: The ERA5 global reanalysis, *Q. J. R. Meteorol. Soc.*, 146, 1999–2049,  
776 <https://doi.org/10.1002/qj.3803>, 2020.

777 Holt, J., Schrum, C., Cannaby, H., Daewel, U., Allen, I., Artioli, Y., et al.: Potential impacts of climate change on the  
778 primary production of regional seas: A comparative analysis of five European seas, *Prog. Oceanogr.*, 140, 91–115, 2016.

779 Holte, J., Talley, L. D., Gilson, J., and Roemmich, D.: An Argo mixed layer climatology and database, *Geophys. Res. Lett.*,  
780 44, 5618–5626, 2017.

781 [Huang J, Pickart RS, Chen Z, Huang RX. 2023. Role of air-sea heat flux on the transformation of Atlantic Water encircling](#)  
782 [the Nordic Seas. \*Nature Communications\* 14: doi:10.1038/s41467-023-35889-3.](#)

783 Ingvaldsen, R. B., Assmann, K. M., Primicerio, R., Fosheim, M., Polyakov, I. V., and Dolgov, A. V.: Physical  
784 manifestations and ecological implications of Arctic Atlantification, *Nat. Rev. Earth Environ.*, 2, 874–889, 2021.

Formatted: Indent: Left: 0 cm

Deleted: ¶

786 Jónsson, S.: The circulation in the northern part of the Denmark Strait and its variability, *ICES CM*, 50, 1999.

787 Jónsson, S., and Briem, J.: Flow of Atlantic water west of Iceland and onto the North Icelandic shelf, 2003.

788 Jónsson, S., and Valdimarsson, H.: Water mass transport variability to the North Icelandic shelf, 1994–2010, *ICES J. Mar.*  
789 *Sci.*, 69, 809–815, <https://doi.org/10.1093/icesjms/fss024>, 2012.

790 Kohler, J., Serra, N., Bryan, F. O., Johnson, B. K., and Stammer, D.: Mechanisms of mixed-layer salinity seasonal  
791 variability in the Indian Ocean, *J. Geophys. Res.-Oceans*, 123, 466–496, 2018.

792 Li, G., Cheng, L., Zhu, J., Trenberth, K. E., Mann, M. E., and Abraham, J. P.: Increasing ocean stratification over the past  
793 half-century, *Nat. Clim. Chang.*, 10, 1116–1123, 2020.

794 Liu, C., Liang, X., Chambers, D. P., and Ponte, R. M.: Global patterns of spatial and temporal variability in salinity from  
795 multiple gridded Argo products, *J. Clim.*, 33, 8751–8766, 2020.

796 Logemann, K., Ólafsson, J., Snorrason, A., Valdimarsson, H., and Marteinsdóttir, G.: The circulation of Icelandic waters  
797 – a modelling study, *Ocean Sci.*, 9, 931–955, 2013.

798 Lozier, M. S., Li, F., Bacon, S., Bahr, F., Bower, A. S., Cunningham, S., et al.: A sea change in our view of overturning in  
799 the subpolar North Atlantic, *Science*, 363, 516–521, 2019.

800 Macrander, A., Valdimarsson, H., and Jonsson, S.: Improved transport estimate of the East Icelandic Current 2002–2012,  
801 *J. Geophys. Res.-Oceans*, 119, 3407–3424, 2014.

802 Mastropole, D., Pickart, R. S., Valdimarsson, H., Våge, K., Jochumsen, K., and Girton, J.: On the hydrography of Denmark  
803 Strait, *J. Geophys. Res.-Oceans*, 122, 306–321, 2017.

804 Mauritzen, C.: Production of dense overflow waters feeding the North Atlantic across the Greenland-Scotland Ridge. Part  
805 1: Evidence for a revised circulation scheme, *Deep-Sea Res. Pt. I*, 43, 769–806, 1996.

806 Moore, G. W. K., Våge, K., Pickart, R. S., & Renfrew, I. A. (2015). Decreasing intensity of open-ocean convection in the  
807 Greenland and Iceland seas. *Nature Climate Change*, 5(9), 877-882.

808 Ólafsson, J.: Winter mixed layer nutrients in the Irminger and Iceland seas, *ICES Mar. Sci. Symp.*, 219, 329–332, 2003.

809 Intergovernmental Panel on Climate Change (IPCC): Special report on the ocean and cryosphere in a changing climate,  
810 2019.

811 Ólafsdóttir, A. H., Utne, K. R., Jacobsen, J. A., Jansen, T., Óskarsson, G. J., Nøttestad, L., Elvarsson, B. Þ., Broms, C.,  
812 and Slotte, A.: Geographical expansion of Northeast Atlantic mackerel (*Scomber scombrus*) in the Nordic Seas from 2007  
813 to 2016 was primarily driven by stock size and constrained by low temperatures, *Deep-Sea Res. Pt. II*, 159, 152–168, 2019.

814 Østerhus, S., Woodgate, R., Valdimarsson, H., Turrell, B., De Steur, L., Quadfasel, D., Olsen, S. M., Moritz, M., Lee, C.  
815 M., Larsen, K. M. H., and Jónsson, S.: Arctic Mediterranean exchanges: a consistent volume budget and trends in transports  
816 from two decades of observations, *Ocean Sci.*, 15, 379–399, 2019.

817 Perez, F. F., Ólafsson, J., Ólafsdóttir, S. R., Fontela, M., and Takahashi, T.: Contrasting drivers and trends of ocean  
818 acidification in the subarctic Atlantic, *Sci. Rep.*, 11, 1–16, 2021.

819 Perez-Hernández, M. D., Pickart, R. S., Torres, D. J., Bahr, F., Sundfjord, A., Ingvaldsen, R., et al.: Structure, transport,  
820 and seasonality of the Atlantic Water boundary current north of Svalbard: Results from a yearlong mooring array, *J.*  
821 *Geophys. Res.-Oceans*, 124, 1679–1698, 2019.

822 Petit, T., Lozier, M. S., Josey, S. A., and Cunningham, S. A.: Atlantic deep water formation occurs primarily in the Iceland

823 Basin and Irminger Sea by local buoyancy forcing, *Geophys. Res. Lett.*, 47, e2020GL091028, 2020.

824 Petit, T., Lozier, M. S., Josey, S. A., and Cunningham, S. A.: Role of air-sea fluxes and ocean surface density on the  
825 production of deep waters in the eastern subpolar gyre of the North Atlantic, *Ocean Sci. Discuss.*, 1–21, 2021.

826 Piron, A., Thierry, V., Mercier, H., and Caniaux, G.: Argo float observations of basin-scale deep convection in the Irminger  
827 Sea during winter 2011–2012, *Deep-Sea Res. Pt. I*, 109, 76–90, 2016.

828 Polyakov, I. V., Pnyushkov, A. V., Alkire, M. B., Ashik, I. M., Baumann, T. M., Carmack, E. C., et al.: Greater role for  
829 Atlantic inflows on sea-ice loss in the Eurasian Basin of the Arctic Ocean, *Science*, 356, 285–291, 2017.

830 Polyakov, I. V., Rippeth, T. P., Fer, I., Alkire, M. B., Baumann, T. M., Carmack, E. C., et al.: Weakening of cold halocline  
831 layer exposes sea ice to oceanic heat in the eastern Arctic Ocean, *J. Clim.*, 33, 8107–8123, 2020.

832 Price, J. F., Weller, R. A., and Pinkel, R.: Diurnal cycling – Observations and models of the upper ocean response to diurnal  
833 heating, cooling, and wind mixing, *J. Geophys. Res.-Oceans*, 91, 8411–8427, 1986.

834 Renfrew, I. A., Pickart, R. S., Våge, K., Moore, G. W., Bracegirdle, T. J., Elvidge, A. D., et al.: The Iceland Greenland  
835 Seas Project, *Bull. Am. Meteorol. Soc.*, 100, 1795–1817, 2019.

836 Reynolds, R. and Banzon, V.: NOAA optimum interpolation 1/4 degree daily sea surface temperature (OISST) analysis,  
837 version 2, NOAA Natl. Cent. Environ. Inf., 10, V5SQ8XB5, 2008.

838 Richardson, K. and Bendtsen, J.: Distinct seasonal primary production patterns in the sub-polar gyre and surrounding seas,  
839 *Front. Mar. Sci.*, 2021.

840 Rudels, B., Björk, G., Nilsson, J., Winsor, P., Lake, I., and Nohr, C.: The interaction between waters from the Arctic Ocean  
841 and the Nordic Seas north of Fram Strait and along the East Greenland Current: Results from the Arctic Ocean-02 Oden  
842 expedition, *J. Mar. Syst.*, 55, 1–30, 2005.

843 Sallée, J.-B., Pellichero, V., Akhoudas, C., Pauthenet, E., Vignes, L., Schmidtko, S., et al.: Summertime increases in upper-  
844 ocean stratification and mixed-layer depth, *Nature*, 591, 592–598, 2021.

845 Sarafanov, A.: On the effect of the North Atlantic Oscillation on temperature and salinity of the subpolar North Atlantic  
846 intermediate and deep waters, *ICES J. Mar. Sci.*, 66, 1448–1454, 2009.

847 Sarmiento, J. L., Hughes, T. M., Stouffer, R. J., and Manabe, S.: Simulated response of the ocean carbon cycle to  
848 anthropogenic climate warming, *Nature*, 393, 245–249, 1998.

849 Semper, S., Våge, K., Pickart, R. S., Valdimarsson, H., Torres, D. J., and Jónsson, S.: The emergence of the North Icelandic  
850 Jet and its evolution from Northeast Iceland to Denmark Strait, *J. Phys. Oceanogr.*, 49, 2499–2521, 2019.

851 Shepherd, J. G., Brewer, P. G., Oschlies, A., and Watson, A. J.: Ocean ventilation and deoxygenation in a warming world:  
852 Introduction and overview, 2017 [Dataset].

853 Skillingstad, E. D., Samelson, R. M., Simmons, H., Laurent, L. S., Merrifield, S., Klenz, T., and Centurioni, L.: Boundary  
854 layer energetics of rapid wind and wave forced mixing events, *J. Phys. Oceanogr.*, 53, 1887–1900, 2023.

855 Stewart, K. D. and Haine, T. W.: Thermobaricity in the transition zones between alpha and beta oceans, *J. Phys. Oceanogr.*,  
856 46, 1805–1821, 2016.

857 Strehl, A.-M., Våge, K., Merdrud, S. L. H., and Barreire, T.: A 70-year perspective on water-mass transformation in the  
858 Greenland Sea: From thermobaric to thermal convection, *Prog. Oceanogr.*, 227, 103304, 2024.

859 Swift, J. H., Aagaard, K., and Malmberg, S.-A.: The contribution of the Denmark Strait overflow to the deep North Atlantic,

860 Deep-Sea Res. Pt. A, 27, 29–42, 1980.

861 Tesdal, J.-E., Abernathy, R. P., Goes, J. I., Gordon, A. L., and Haine, T. W.: Salinity trends within the upper layers of the  
862 subpolar North Atlantic, *J. Clim.*, 31, 2675–2698, 2018.

863 Valdimarsson, H., Astthórsson, O. S., and Pálsson, J.: Hydrographic variability in Icelandic waters during recent decades  
864 and related changes in distribution of some fish species, *ICES J. Mar. Sci.*, 69, 816–  
865 825, <https://doi.org/10.1093/icesjms/fss027>, 2012.

866 Våge, K., Moore, G. W. K., Jónsson, S., and Valdimarsson, H.: Water mass transformation in the Iceland Sea, *Deep-Sea*  
867 *Res. Pt. I*, 101, 98–109, 2015.

868 Våge, K., Papritz, L., Havik, L., Spall, M. A., and Moore, G. W. K.: Ocean convection linked to the recent ice edge retreat  
869 along East Greenland, *Nat. Commun.*, 9, 1–8, 2018.

870 Våge, K., Pickart, R. S., Moore, G., and Ribergaard, M. H.: Winter mixed layer development in the central Irminger Sea:  
871 The effect of strong, intermittent wind events, *J. Phys. Oceanogr.*, 38, 541–565, 2008.

872 Våge, K., Pickart, R. S., Spall, M. A., Moore, G., Valdimarsson, H., Torres, D. J., et al.: Revised circulation scheme north  
873 of the Denmark Strait, *Deep-Sea Res. Pt. I*, 79, 20–39, 2013.

874 Våge, K., Pickart, R. S., Spall, M. A., Valdimarsson, H., Jónsson, S., Torres, D. J., et al.: Significant role of the North  
875 Icelandic Jet in the formation of Denmark Strait Overflow Water, *Nat. Geosci.*, 4, 723–727, 2011.

876 Våge, K., Semper, S., Valdimarsson, H., Jónsson, S., Pickart, R. S., & Moore, G. W. K. (2022). Water mass transformation  
877 in the Iceland Sea: Contrasting two winters separated by four decades. *Deep Sea Research Part I: Oceanographic Research*  
878 *Papers*, 186, 103824.

879 Whitney, M. M. (2025). Icelandic riverine freshwater distribution, offshore export, and alongshelf connectivity. *Estuarine,*  
880 *Coastal and Shelf Science*, 319, 109266.

881 Yamaguchi, R. and Suga, T.: Trend and variability in global upper-ocean stratification since the 1960s, *J. Geophys. Res.-*  
882 *Oceans*, 124, 8933–8948, 2019.

883

884



Page 14: [2] Formatted Angel Ruiz Angulo - HI 10/03/2026 22:27:00

Font: Not Italic

Page 14: [2] Formatted Angel Ruiz Angulo - HI 10/03/2026 22:27:00

Font: Not Italic

Page 14: [2] Formatted Angel Ruiz Angulo - HI 10/03/2026 22:27:00

Font: Not Italic

Page 14: [2] Formatted Angel Ruiz Angulo - HI 10/03/2026 22:27:00

Font: Not Italic

Page 14: [2] Formatted Angel Ruiz Angulo - HI 10/03/2026 22:27:00

Font: Not Italic

Page 14: [2] Formatted Angel Ruiz Angulo - HI 10/03/2026 22:27:00

Font: Not Italic

Page 14: [2] Formatted Angel Ruiz Angulo - HI 10/03/2026 22:27:00

Font: Not Italic

Page 14: [2] Formatted Angel Ruiz Angulo - HI 10/03/2026 22:27:00

Font: Not Italic

Page 14: [2] Formatted Angel Ruiz Angulo - HI 10/03/2026 22:27:00

Font: Not Italic

Page 14: [2] Formatted Angel Ruiz Angulo - HI 10/03/2026 22:27:00

Font: Not Italic

Page 14: [2] Formatted Angel Ruiz Angulo - HI 10/03/2026 22:27:00

Font: Not Italic

Page 14: [3] Deleted Angel Ruiz Angulo - HI 10/03/2026 21:28:00

Page 14: [3] Deleted Angel Ruiz Angulo - HI 10/03/2026 21:28:00

Page 19: [4] Deleted Angel Ruiz Angulo - HI 09/03/2026 16:50:00